Available online at www.sciencedirect.com
SCIENCE DIRECT
Journal of Magnetic Resonance 178 (2006) 96–105
JMR Journal of Magnetic Resonance
www.elsevier.com/locate/jmr

Sample patterning on NMR surface microcoils

K. Ehrmann [a,*], M. Gersbach [a], P. Pascoal [b], F. Vincent [a], C. Massin [a], D. Stamou [c], P.-A. Besse [a], H. Vogel [b], R.S. Popovic [a]

[a] Institute of Microsystems, EPFL—Ecole Polytechnique Fédérale de Lausanne, CH–1015 Lausanne, Switzerland
[b] Institute of Chemical Engineering, EPFL—Ecole Polytechnique Fédérale de Lausanne, CH–1015 Lausanne, Switzerland
[c] Bio-Nanotechnology Laboratory, Nano-Science Center, University of Copenhagen, Universitetsparken 5, DK-2100 Copenhagen, Denmark

Received 1 June 2005; revised 8 August 2005
Available online 18 October 2005

Abstract

Aligned microcontact printing for patterning the sample in areas of homogeneous RF-field on the highly sensitive surface of planar NMR microprobes is presented. We experimentally demonstrate that sample patterning allows drastic improvement of the spin excitation uniformity. The NMR microprobes are designed for cell analysis and characterized using lipid vesicles as cell substitutes. Lipid vesicles are advantageous as composition and concentration of the confined solution are precisely controlled and because of their similarity to living cells. Using aligned microcontact printing, a monolayer of lipid vesicles is immobilized on the surface of the planar NMR microprobe in a patterned way. ^{1}H NMR spectra and CPMG spin echoes of sucrose solution confined within the lipid vesicles are successfully recorded. Nutation curves of the sample structured in different patterns demonstrate the impact of patterning on the spin excitation uniformity. The total detection volumes are between 1 and 2 nL and derived with help of a theoretic model based on 3D finite element simulation. This model predicts the signal-to-noise ratio and the progression of the nutation curves.

Keywords: Planar surface microcoil; B_1 homogeneity; Signal-to-noise ratio; Lipid vesicles; Aligned microcontact printing

1. Introduction

There is a growing interest in the manipulation and analysis of cells in small quantities down to single cells. Especially micro- and nano-engineering techniques, which offer new possibilities for cell manipulation and analysis, have stimulated the progress in this field [1]. When analyzing living cells, mostly electrical (impedance) and optical (fluorescent) characterization techniques are used.

Nuclear magnetic resonance is an information rich analysis technique that brings about a lot of potential for new insights and applications in cell analysis [2,3]. Performing NMR analysis of living cells, the cell handling is a very delicate issue. The cells are generally extracted from living tissue or harvested from their cultivation environment in bioreactors or on the surface of Petri dishes or well plates. Due to the principally 2D morphology of living cells, planar coils, where the cells could be directly immobilized or grown on the coil surface, should be better suited for analysis than conventional solenoidal coils, where the sample is confined in the volume of a capillary or tube. Small planar coils can be produced by microfabrication. In addition to the advantages of exact reproducibility and batch-production, microfabrication allows producing extremely small and highly sensitive microcoils for spectroscopy of mass-limited samples and high-resolution imaging.

Planar, microfabricated coils on a GaAs substrate for NMR analysis have been developed first by Peck et al. [4,5]. Trumbull et al. [6] have tried to integrate CE separation and NMR spectroscopy following the concept of micro total analysis systems. Previously, we have optimized the design of planar microcoils for high sensitivity and integrated microfluidic channels in the glass substrate

* Corresponding author. Fax: +41 21 693 6670.
E-mail address: klaus.ehrmann@epfl.ch (K. Ehrmann).

1090-7807/$ - see front matter © 2005 Elsevier Inc. All rights reserved.
doi:10.1016/j.jmr.2005.08.018

[7]. As the focus of these experiments was on chemical analysis, planar microprobes were used confining the sample in a capillary or microchannel instead of using directly the surface of the planar microcoil as sample interface. Besides the aptitude to the analysis of living cells, placing the sample on the surface of the microcoil does not require complicated channel fabrication and allows sample positioning close to the microcoil. This is especially important when using very small microcoils with a limited sensitive region.

Eroglu and Gimi [8] have placed an acrylic container with a flat bottom onto a planar microcoil of 1.5 mm inner diameter. Images of pancreatic rat islets placed in this container have been taken [9]. Due to the inhomogeneous RF-field close to the planar microcoil [10], a compromise had to be made between spin excitation uniformity and sensitivity. The strong RF-field near the coil increases the sensitivity, but the inhomogeneity of the field causes low spin excitation uniformity.

In this contribution, we present the application of a micro-engineering technique to pattern the sample in areas of homogenous RF-field on the microprobe surface close to the NMR microcoil for an improved compromise between spin excitation uniformity and high sensitivity. The microfabricated NMR probe imitates a Petri dish, because integrated cell growing and NMR spectroscopy and imaging of living cells is aimed finally (see Fig. 1).

As the volume of the cells immobilized on the microprobe surface and the concentrations of the various compounds within living cells are not precisely controlled, lipid vesicles that contain a sucrose solution of known concentration are used as cell substitutes to characterize the surface microcoil with respect to sensitivity and spin excitation uniformity. Monolayers of these vesicles are immobilized in different patterns on the microprobe surface. The advantage of using lipid vesicles is, beside the controlled contents, their long-time stability and the similarity to living cells with respect to immobilization techniques and perturbation of the static magnetic field ($\mathbf{B}_0$-field). Knowing the sample concentration, a theoretical model based on finite element simulation of the microcoil's inhomogeneous RF-field is used to calculate the volume of the vesicles and to predict sensitivity and spin excitation uniformity of different sample patterns.

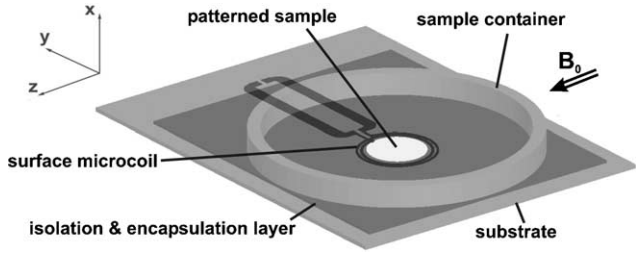

Fig. 1. Design of the NMR surface microcoil with a sample container on top imitating a petri dish. The microcoil has an inner diameter of 1 mm. The sample is patterned in the center of the microprobe surface. The microprobe is introduced into the NMR magnet such that the static magnetic $\mathbf{B}_0$-field lies in the z-direction.

2. Theory

2.1. Theoretic model

We determine sensitivity through the *SNR* produced by an average spin flip angle of 90°. Spin excitation uniformity is quantified by the percentage of the *SNR* produced by a 450° compared to the *SNR* produced by a 90° flip angle. The theoretic model computes the nutation curve of a given coil-sample-configuration according to Eq. (1). We described the derivation of this equation in a previous contribution [7]. The model here is extended to return the final *SNR* monitored by the spectrometer.

$$SNR(\tau_{ex}) = \frac{S(\tau_{ex})}{\sqrt{4kTR_{coil}}} \cdot \sqrt{n_{acq}} \cdot \frac{1}{F'} \cdot \frac{T_2^*}{\sqrt{2T_{acq}}} \tag{1}$$

$S(\tau_{ex})$ denotes the detection signal amplitude dependent on the excitation time τ_{ex}, k is the Boltzman constant, T is the coil's temperature, R_{coil} is the coil's electrical resistance and n_{acq} is the number of acquisitions. F' is the noise factor of the detection electronics, T_2^* is the apparent spin–spin relaxation time and T_{acq} is the acquisition time.

The signal amplitude $S(\tau_{ex})$ is calculated according to the principle of reciprocity [11] by integration of the signal amplitude per unity volume of each point in space $S(\mathbf{r}, \tau_{ex})$ over the whole sample volume V_s:

$$S(\tau_{ex}) = \int_{V_s} S(\mathbf{r}, \tau_{ex}) \mathrm{d}V_s \tag{2}$$

with

$$S(\mathbf{r}, \tau_{ex}) = \omega_0 \cdot M_0 \cdot B_{1u,xy}(\mathbf{r}) \cdot \sin\left(\gamma \cdot \frac{I_{ex}}{2} \cdot \tau_{ex} \cdot B_{1u,xy}(\mathbf{r})\right) \tag{3}$$

ω_0 denotes Larmor frequency and M_0 is the net magnetization of the sample. $B_{1u,xy}(\mathbf{r})$ is the magnitude of the unitary magnetic field ($\mathbf{B}_1$-field) in the xy-plane, γ is the gyromagnetic constant of the excited nuclei and I_{ex} the excitation current.

As the $\mathbf{B}_1$-field is considered in the detection and excitation modeling, the exact progression of the nutation curve can be determined, if the inhomogeneity of the $\mathbf{B}_1$-field is precisely assessed. In a completely homogeneous $\mathbf{B}_1$-field, the nutation curve is an ideal sinusoidal function. In an inhomogeneous $\mathbf{B}_1$-field, the nutation curve is a superposition of sinusoidal functions with different rotation frequencies. This superposition results in a curve, which looses its sinusoidal behavior for high excitation times, as the spins' rotation frequencies disperse. The more inhomogeneous the $\mathbf{B}_1$-field, the faster is the dispersion and the smaller the *SNR* of a 450° excitation with respect to the *SNR* of a 90° excitation.

An elegant way to obtain the precise $\mathbf{B}_1$-field is the use of finite element simulation. The 3D geometry of our microcoil is automatically generated based on the mask layout and a technology process file (MEMS Pro, Memscap). It is imported into the finite element simulation program (Maxwell 3D, Ansoft), where the sample geometry is added. An eddy current analysis returns the 3D unitary $\mathbf{B}_1$-field. The simulation program handles arbitrary coil-sample configurations.

The noise factor F' introduced in Eq. (1) or the equivalent noise figure $F(\mathrm{d}B)$ ($F' = 10^{F/20}$) of the detection electronics comprises the attenuation of the PCB (printed circuit board) A_{PCB}, the attenuation of the cable from the PCB to the conventional spectrometer A_{cable} and the noise figure of the spectrometer F_{spec}:

$$F = A_{\mathrm{PCB}} + A_{\mathrm{cable}} + F_{\mathrm{spec}}. \tag{4}$$

The recent model cannot predict the perturbations of the $\mathbf{B}_0$-field and consequently T_2^* can only be estimated. For comparison with experiments, T_2^* is calculated from the measured linewidth LW (FWHM):

$$T_2^* = \frac{1}{\pi \cdot LW}. \tag{5}$$

This T_2^* is then included in the model.

2.2. Sensitivity and spin excitation uniformity on microcoil surface

Since this contribution focuses on the patterning of the sample, all presented experiments are performed with microcoils of identical geometry (see Fig. 2). The distance of 10 μm from the microcoil turns to the microprobe surface is very small compared to the coil diameter of 1 mm and consequently the sensitivity is very high on the probe surface [10]. The microprobe is inserted into the magnet such that the $\mathbf{B}_0$-field is parallel to the probe surface (see Fig. 1).

Sensitivity and spin excitation uniformity for different sample geometries and positions can be computed with the theoretic model. The sample is modeled as a homogeneous water layer with a layer height of 10 μm. Because of the rotational symmetry of $B_{1\mathrm{u},xy}(\mathbf{r})$, the modeled sample patterns have circular shape and are centered with respect to the microcoil center. Fig. 3 shows computed sensitivity and spin excitation uniformity of circular sample patterns with different diameters. It can be seen that the sensitivity is increasing almost proportional with the sample volume as long as the sample is within the microcoil turns (diameter <1000 μm). The spin excitation uniformity is very good for small sample diameters and falls drastically for sample diameters larger than half the coil diameter (>500 μm). If the sample exceeds the microcoil turns, the spin excitation uniformity cannot be determined correctly any more (dotted line), because the sinusoidal behavior of the nutation curve gets completely lost.

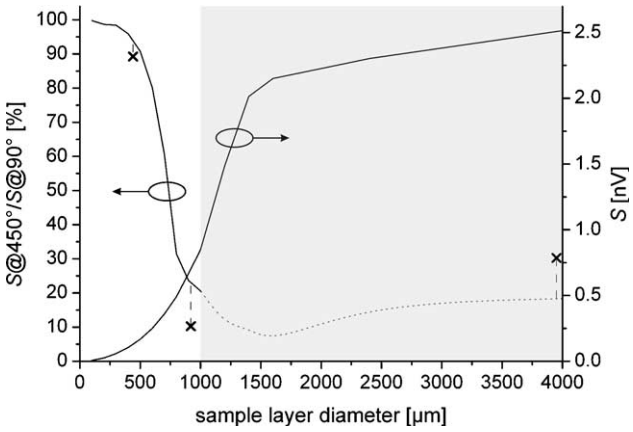

Fig. 3. Model prediction of sensitivity (S) and spin excitation uniformity (S@450°/S@90°) using a microcoil with 1000 μm inner diameter. The sample is modeled as a circular water layer of 10 μm height with variable diameter placed on the microprobe surface. If the sample layer diameter is greater than 1000 μm, sample is also placed on the surface above the coil turns (gray part of graph). Then the spin excitation uniformity can hardly be determined because the nutation plots loose their sinusoidal behavior (dashed spin excitation uniformity curve). **x** indicates experimentally realized sample patterns and the measured spin excitation uniformity.

3. Experimental

3.1. Microprobe fabrication

The planar surface microcoils are batch-fabricated on 4-inch glass wafer substrates in five photolithographic steps (see also [12]). The coil pads are electroplated in Cu on a Cr–Cu-seedlayer that is evaporated on Pyrex glass wafers. Electroplating is done to a pad height of 10 μm in a mould of SJR (Shipley Microposit 5000 series). A 15 μm thick SU-8 photo-epoxy layer (Microchem 2000 series) serves as isolation between coil pads and coil turns. Onto the structured SU-8, a second Cr–Cu-seedlayer is evaporated for electroplating the coil turns to a height of 15 μm. Having finished the electroplating, the seedlayers are etched away and the microcoils are encapsulated using a SU-8 layer of 25 μm, which results in a distance of 10 μm from the coil turns to the microprobe surface. The encapsulation effects a

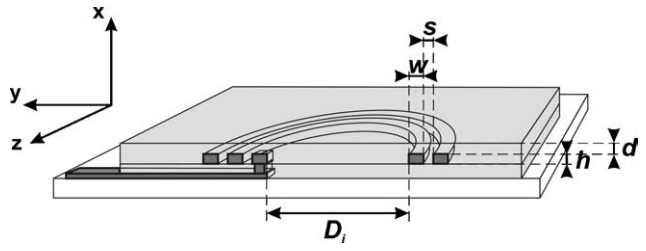

Fig. 2. Scheme of microcoil with cross-section in the xy-plane through the coil center. The microcoils used in all experiments have two turns, an inner diameter (D_i) of 1 mm, a turn width (w) of 40 μm, a space (s) between the turns of 30 μm, a coil turn height (h) of 15 μm and a distance (d) between the microcoil turns and the microprobe surface due to the encapsulation of 10 μm.

smooth and planar microprobe surface and avoids short circuits of the coil turns when attaching the sample directly on top of the coil.

The fabricated microcoils are electrically characterized by a HP impedance analyzer and coplanar RF probes (Picoprobes, GGB Industries). The underlying electrical model for the microcoil is an inductor in series with a resistance. All coils have a resistance R_{coil} of 0.68 Ω at 300 MHz and an inductance L_{coil} of 10.7 nH.

The detection resonance circuit is implemented on a PCB to which the diced microcoil chip is glued and bonded. The circuit is tuned and matched to 50 Ω at 300 MHz using two trimmer capacitors (CTZ3 series, AVX) such that the microprobe can be connected to the preamplifier of a conventional NMR spectrometer.

The PCB is fixed to a special probe base, which is milled to enter into the shimming system of a narrow bore superconducting magnet.

A PMMA cylinder is glued on top of the SU-8 surface of the microcoil. It serves as a sample container similar to a Petri dish. The cylinder has an inner diameter of 5 mm and a height 0.5 mm. It is chosen as flat and large as possible to minimize the perturbations of the $\mathbf{B}_0$-field (see [7]) and to place the detection volume of the microcoil away from the strongly perturbed regions at the borders of the cylinder. Fig. 4 shows one of the microfabricated coils with the sample container glued on top and bonded to the PCB.

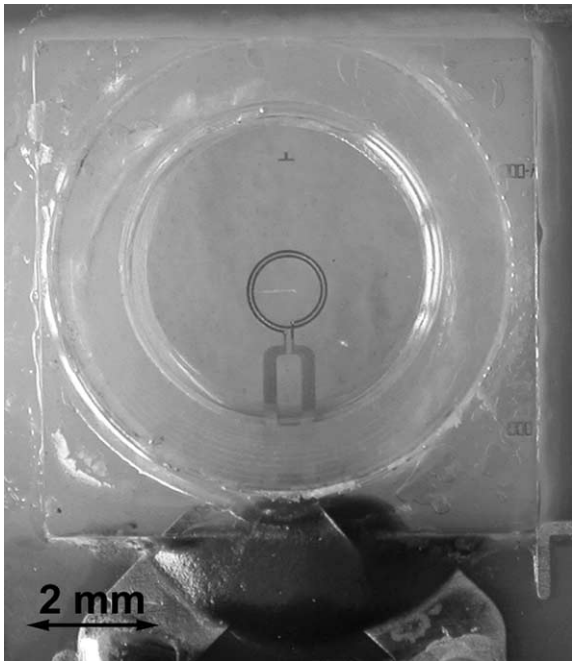

Fig. 4. Picture of the fabricated surface microcoil with the sample container glued on top of the SU-8 encapsulation layer. The pads of the microcoil pass underneath the container and are wire-bonded to the PCB.

3.2. Lipid vesicles as cell substitutes

Lipid vesicles, also called liposomes, consist of amphiphilic molecules that self-assemble in aqueous solution to bilayer membrane spheres. Different types of amphiphilic molecules can be mixed and amphiphilic molecules conjugated with other functional molecules can be added. This allows tailoring the properties of lipid vesicles for a great variety of applications. They can, for example, be used as attolitre containers and molecular shuttles [13] or for rapid diffusion mixing when studying chemical reaction [14]. Others have used lipid vesicles as cell model systems emulating the formation, growth, and division of living cells [15].

Here, lipid vesicles are used as cell substitutes because of their advantageous features for the quantification of the microprobe sensitivity: Composition and concentration of the solution confined in lipid vesicles is precisely controlled, as the solution is prepared separately. Unlike living cells, which exchange compounds with the exterior, the solution within lipid vesicles is stable for long times. Form, size, and membrane of the vesicles are very similar to that of living cells. Therefore, the perturbations of the $\mathbf{B}_0$-field are expected to be the same. The almost identical membrane allows furthermore using the same immobilization and patterning techniques for both samples.

We take phospholipids, which are the amphiphilic molecules that form the membranes of living cells, to create the vesicles. The main lipid DOPG (1,2-dioleoyl-*sn*-glycero-3[phospho-rac-(1-glycerol)]), 0.3% of DSPE-PEG_{2000} biotin (1,2-distearoyl-*sn*-glycero-3-phosphoethanolamine-*N*-[biotinyl(polyethylene glycol) 2000) for the immobilization, and 0.1% of TRITC DHPE (N-(6- tetramethylrhodaminethiocarbamoyl)-1,2-dihexadecanoyl-*sn*-glycero-3-Phosphoethanolamine) for fluorescent detection are mixed in their chloroform solution. After mixing, the chloroform is evaporated and 1 M sucrose in deuterated PBS (phosphate-buffered saline) is added. The lipids self-assemble to bilayers and form vesicle spheres with sizes up to 30 μm diameter that confine the sucrose solution. The lipid vesicles are filtered using 0.8 M sodium chloride solution in deuterated PBS. Thereby, only vesicles with a diameter bigger than 3 μm are kept, the sucrose solution is only within the vesicles and the osmotic pressure is equilibrated.

3.3. Sample immobilization and patterning

The lipid vesicles immobilize on the microprobe surface by high affinity interactions between biotin, a ligand conjugated to the vesicles and neutravidin, a receptor molecule incubated on the microprobe surface. Because of the highly specific binding interactions between biotin and neutravidin, the vesicles can be patterned on the microprobe surface. They immobilize only on areas that are incubated with neutravidin. Fig. 5 illustrates this concept.

We use microcontact printing for the patterned incubation of neutravidin because of its easy application and flexibility. Microcontact printing was first developed by the

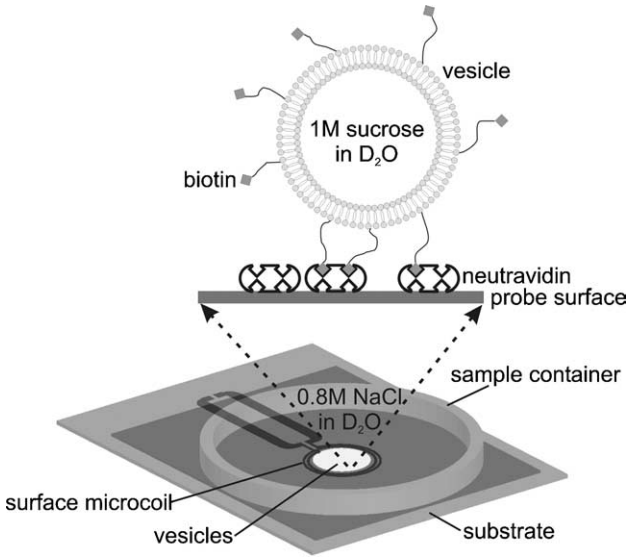

Fig. 5. Design illustrating the concept of vesicle immobilization on the microprobe surface. The lipid vesicles are conjugated with biotin that specifically binds to neutravidin patterned by aligned microcontact printing onto the microprobe surface.

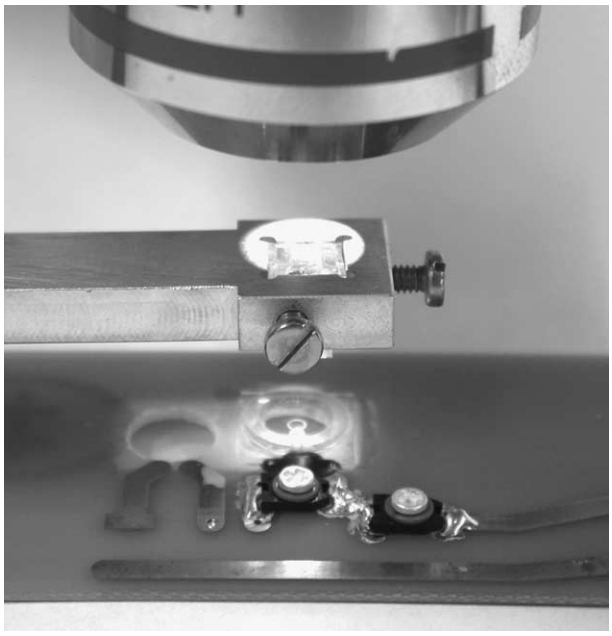

Fig. 6. Picture of the setup for aligned microcontact-printing. The PDMS stamp is attached to the milled arm of a micromanipulator. The microcoil chip is glued and wire-bonded to a PCB. The alignment is done under an optical microscope.

group of Whitesides [16] for patterning thiolalkane molecules on gold surfaces. Since then it has been extended for patterning a variety of molecules [17] and nano-objects. An elastomeric stamp, which contains a micro-engineered surface relief, is incubated with a molecule of choice that is transferred from the stamp to the surface only in the regions of conformal contact.

The stamps for microcontact printing are cast from the mold of a microfabricated master with the negative relief. On a 4-inch silicon wafer, 80 μm of SU-8 (1060, Gerstel) is spun and structured using photolithography. The master is then silanized to make the surface hydrophobic and to facilitate the detachment of the stamp. PDMS (polydimethylsiloxane, Sylgard 184, Dow Corning) is poured onto the structures of the master until the desired stamp thickness of ~1 cm is achieved and subsequently polymerized at 80 °C for 2 h. After detaching the PDMS layer from the master, it is cut to the individual stamps.

To pattern with respect to an underlying surface structure, aligned microcontact printing is used [18,19]. In our setup, the stamp is fixed to a micromanipulator using a milled arm. The NMR microprobe and the stamp are approached to each other under a light-field microscope. Fig. 6 shows the setup for aligned microcontact printing.

When patterning lipid vesicles, neutravidin is incubated on the PDMS stamp in a PBS solution. Then the neutravidin is printed to the microcoil surface using the alignment setup. The lipid vesicles in sodium chloride PBS solution are added and a monolayer immobilizes on the neutravidin in form of the respective pattern. The non-immobilized vesicles are carefully rinsed away. The sample container is finally filled with sodium chloride solution in deuterated PBS and closed using an adhesive film (Falcon, BD). The pattern of the immobilized vesicles is verified with a confocal microscope. All NMR experiments are performed with a conventional NMR spectrometer and a 7 T narrow bore superconducting magnet (Bruker DRX 300).

4. Results

4.1. Calibration with macro sample container

The difference between measured and theoretic *SNR* is assumed to be a constant factor throughout all experiments caused by non-considered additional losses in the detection electronics. In a calibration experiment with a known sample volume, this ratio is assessed and introduced into the calibrated model as an additional attenuation.

The calibration experiment is performed by taking spectra of water confined in the sample container. The measurements return a *SNR* of 4700 for a 90° average excitation flip angle.

The computed signal amplitude S, according to Eqs. (2) and (3), of water in the sample container is 36.6 μV ($\omega_0 = 2\pi$ 300 MHz, $M_0 = 22$ mA/m, $I_{ex} = 460$ mA and $\tau_{ex} = 10$ μs). The theoretical noise due to the resistance of the microcoil is 0.11 nV/$\sqrt{\text{Hz}}$. Attenuation simulation (ADS, Agilent) of the electronic circuit on the PCB (see Fig. 7) including bonding wires of 0.2 Ω resistance and 1 nH inductance each (Philips/TU Delft Model [20]) and tuning and matching capacitors with a Q-factor of 100 at 300 MHz returned A_{PCB} of 2.9 dB. The cable has an attenuation A_{cable} of 0.54 dB. Estimating 1 dB for the noise figure of the spectrometer electronics F_{spec}, the total noise figure F adds up to 4.4 dB (according to Eq. (4)).

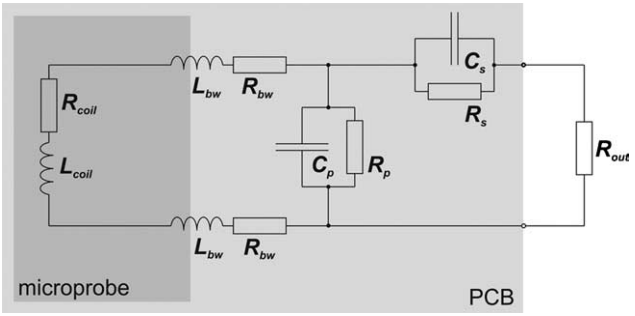

Fig. 7. Scheme of electrical circuit used for attenuation simulation. L_{bw} and R_{bw} are the inductance and resistance of the bonding wires. C_p, C_s and R_p, R_s are the capacitances and the losses of the capacitors used for tuning and matching. R_{out} depicts the 50 Ω impedance of the subsequent electronics.

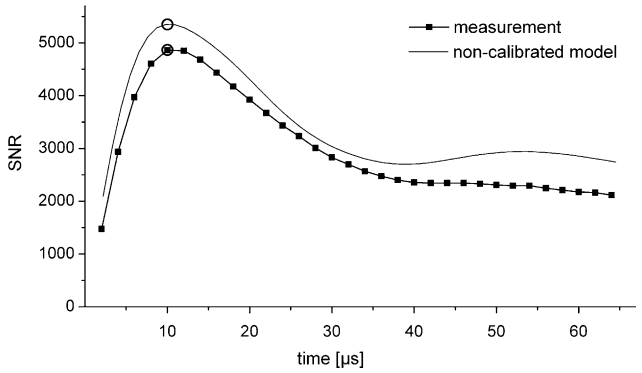

Fig. 8. Measured and modeled nutation curve of water in sample container. The *SNR*s at a 90° average excitation flip angle used for calibration are highlighted.

The measured linewidth *LW*, needed for calculating the *SNR* after Fourier transformation, is 4.3 Hz. This linewidth is equivalent to a T_2^* of 75 ms. According to literature, the spin–spin relaxation time T_2 of water is 2.8 s [21]. The major source of this linewidth broadening is the perturbation of the $\mathbf{B}_0$-field caused by the sample container. In consideration of these values, the model returns a final *SNR* in frequency domain of 5300 after one acquisition and 4 s acquisition time. This result is only 13% higher than the measured *SNR* and means that 1 dB of additional attenuation must be introduced into the calibrated model. Fig. 8 shows the measured and modeled nutation curve of the calibration experiment.

4.2. Vesicle patterns and spin excitation uniformity

To show the feasibility of sample patterning, its influence on the NMR performance and especially the improvement of the spin excitation uniformity, three different vesicle patterns are structured on the surface of the microprobe (see Fig. 9). In pattern (A), the vesicles are homogeneously distributed on the whole surface. Pattern (B) avoids having the vesicles above the microcoil turns where the $\mathbf{B}_1$-field is most inhomogeneous. In pattern (C), the vesicles are only structured in the very center of the microcoil surface, where the $\mathbf{B}_1$-field is very homogeneous. As the vesicle area is very small in pattern (C), several layers of vesicles are deposited by performing several, subsequent immobilization steps. Due to the high salt concentration, the vesicles stick to each other and after the immobilization of a first monolayer to the neutravidin, adding new vesicles

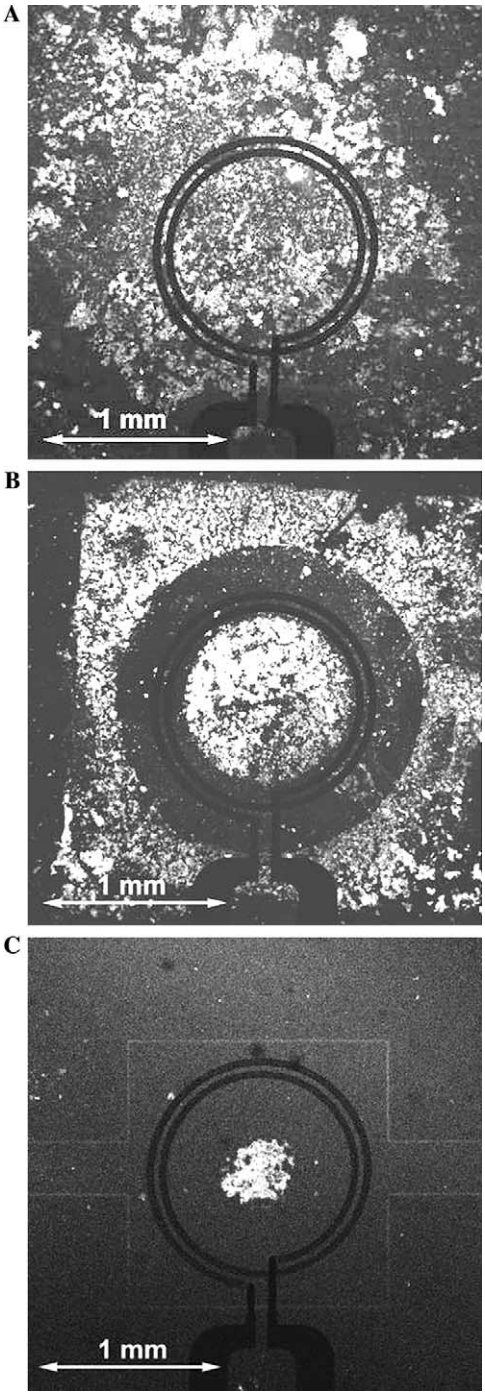

Fig. 9. Fluorescent images of the vesicle patterns taken with a confocal microscope. The microcoil appears black because of the opaque copper lines. The vesicles are labelled with rhodamin and appear white. They are immobilized in pattern (A), (B), and (C). The diameter of the vesicle area in pattern (B) is 920 μm and in pattern (C) it is 440 μm.

increases the amount of vesicles on the patterned areas. Thereby, the decreased sample surface is compensated by an increased average sample height and the loss in detection volume is reduced.

In the finite element simulation, the vesicle volume is modeled as a flat circular sample layer placed directly on the microprobe surface. The height of the layer is chosen such that the *SNR* of the calibrated model is equal to the measured *SNR* at a 90° excitation. The measured linewidth of the sucrose peaks needed for the calculation of the *SNR* in frequency domain is 15 Hz at all three patterns and corresponds to a T_2^* of 21 ms. The linewidth broadening with respect to 4.3 Hz of water in the sample container, could be due to the static magnetic field perturbations of the vesicles itself. The influence of the proximity to the copper turns seems to be negligible, as patterns (A), (B) and (C) have different distances from the sample to the coil turns but show the same linewidth. The biggest peak in the sucrose spectrum, the H-6 peak, originates from the resonance of the two H-6 protons in the glucose ring and the two H-6 protons in the fructose ring and is located at 3.8 ppm. Fig. 10 shows the measured and modeled nutation curves of the H-6 peak of sucrose with the vesicles patterned according to Fig. 9. At each excitation time, the *SNR* of the H-6 proton peak after 512 acquisitions is taken. As expected, pattern (A) returns very bad spin excitation uniformity. The nutation curve shows that a 180° flip angle excitation, which should return zero signal, is not possible. The spin excitation uniformity can be increased, when avoiding the surface directly on top of the microcoil turns. In contrast to pattern (A), pattern (B) clearly shows sinusoidal oscillation. An almost perfect sinusoidal behavior is obtained if the sample is placed only in the very center of the microcoil like in pattern (C). A 450° flip angle excitation returns a *SNR* of 90% of the *SNR* at a 90° flip angle excitation. Table 1 gives an overview to the most important results of the presented experiments.

4.3. Sensitivity and limit of detection

Sensitivity and limit of detection are evaluated by taking spectra of sucrose confined within the lipid vesicles that are immobilized on the microprobe surface according to pattern (C). Fig. 11 shows the spectrum of sucrose after 512 acquisitions. Despite water suppression by pre-saturation, the spectrum contains a big water peak, which is caused by the water residues in deuterated water. The measured SNR of the H-6 peak is 9 after 512 acquisitions. The SNR of the peak at 5.4 ppm that originates from the anomeric proton in the sucrose molecule is ~2.

A method to increase the *SNR* is the application of a weighting function of exponential decay, which causes *LB* of additional Lorentzian broadening. Maximum *SNR* is obtained with $LB = LW$. If the acquisition time T_{acq} is much greater than $(\pi(LW + LB))^{-1}$, T_{acq} in Eq. (1) can be replaced by T_2^* [22,23]. In our case, the result is a theoretically five-fold increase of the *SNR*. Measurement after Lorentzian broadening returns *SNR*s of the H-6 peak and the anomeric proton peak of 45 and 10, respectively.

The total acquisition time doing 512 acquisitions, with a pre-saturation time of 3 s and an acquisition and waiting time of 4 s, is 1 h. Defining the limit of detection at a *SNR* of 3 within 1 h, the minimal detectable concentration (LOD_c) of molecules with one equivalent proton is

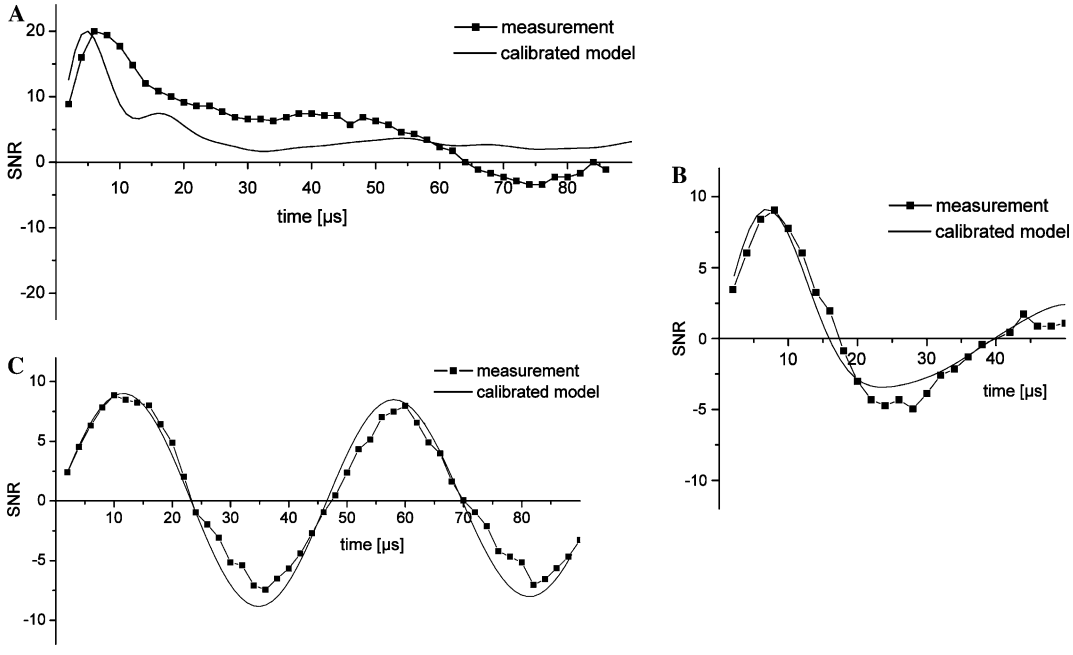

Fig. 10. Measured and modeled nutation curves of the H-6 peak of sucrose confined within vesicles that are structured according to the patterns in Fig. 9. The total detection volumes are 1.9, 1.0, and 1.2 nL for the patterns (A), (B), and (C), respectively.

Table 1
Performance characteristics of the calibration experiment using water in the sample container and of the patterning experiments having sucrose confined within vesicles that are structured in pattern (A), (B) and (C) on the microprobe surface

	Detection volume (nL)	Measured LW (Hz)	Measured SNR ($n_{acq} = 512$)	Measured $S@450°/S@90°$ [%]
Water in sample container	900	4.3	4700 ($n_{acq} = 1$)	—
Sucrose (H-6 peak) in vesicle—pattern (A)	1.9	15	20	(30)[a]
Sucrose (H-6 peak) in vesicle—pattern (B)	1.0	15	9	10
Sucrose (H-6 peak) in vesicle—pattern (C)	1.2[b]	15	9	90

[a] Pattern (A) does not show sinusoidal behavior and therefore $S@450°/S@90°$ cannot be taken as a reliable indicator for spin excitation uniformity.
[b] The relative big volume of pattern (C) is due to the increased sample height realized by several vesicle immobilization steps.

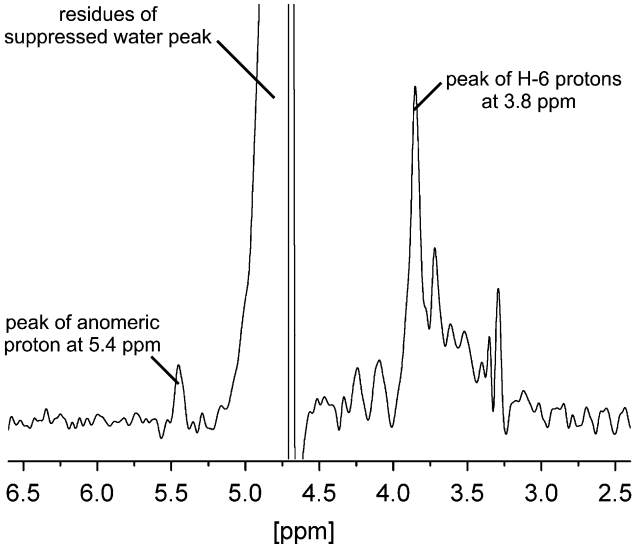

Fig. 11. ^{1}H spectrum of sucrose confined in vesicles immobilized according to pattern (C) on the microcoil surface. The signal to noise ratios of the H-6 peak and the anomeric proton peak are 9 and ~2, respectively, after 512 acquisitions without signal treatment. The original FID data is multiplied by a Lorentz–Gauss weighting function $h(t) = e^{(t/T_2^* - \sigma^2 t^2/2)}$, with $T_2^* = 21$ ms and $\sigma^2 = 1180$. The resulting spectrum has a Gaussian lineshape with a linewidth of ~13 Hz [23]. The baseline is corrected.

300 mM. The total acquisition time could be increased, as experiments several days after the vesicle immobilization returned the same signal magnitude, meaning that the sucrose is well confined within the vesicles.

4.4. Spin echo train

Patterning the sample in the homogenous regions of the microprobe surface produces excellent spin excitation uniformity and permits more advanced excitation pulse sequences like, for example, spin echo trains. After structuring the lipid vesicles on the microcoil surface according to pattern (C), a CPMG (Carr–Purcell–Meiboom–Gill) spin echo train is performed. The time between the echoes is set to 20 ms. The sucrose spectra of every second echo are recorded with 2048 acquisitions each. Fig. 12 shows the initial sucrose spectrum in the foreground and every second spectrum of the 10 following echoes.

5. Discussion

5.1. Performance of the NMR surface microcoil

In this contribution, a technology that allows patterning the sample on the surface of NMR microprobes very close to the planar microcoil is presented. A high contrast between patterned and non-pattern areas is achieved. NMR spectroscopy results clearly show the improvement of the spin excitation uniformity when the sample is patterned in areas of more and more homogenous $\mathbf{B}_1$-field. Restricting the sample according to pattern (C) in the center of the microcoil, a 450° spin flip angle excitation returns 90% signal magnitude with respect to a 90° flip angle excitation. This is in the range of standard solenoidal or saddle coils and permits performing complex pulse sequences. For demonstration, a series of CPMG spin echo is recorded.

Conventional analytic models for the prediction of NMR performance contain only partial information about the $\mathbf{B}_1$-field inhomogeneity and are hardly applicable to planar coils. We use a model that is based on 3D finite element simulation of the $\mathbf{B}_1$-field. The consideration of the exact coil geometry and the precise computation of the spatial $\mathbf{B}_1$-field allow determining the coil's sensitive region and the deterioration of spin excitation uniformity in inhomogeneous $\mathbf{B}_1$-fields. The modeled progressions of the nutation curves match the measured ones very well for all patterns (see Fig. 10). The difference between modeled SNR prediction and measurement result is only 13%. The rough estimation of the noise figure in the spectrometer electronics and the neglecting of additional loss sources might be the reason for this difference.

We saw, that when patterning the sample in homogeneous $\mathbf{B}_1$-field areas on the microprobe surface, the compromise between spin excitation uniformity and sensitivity is improved, but not completely eliminated (Fig. 3). The applied patterning technique allows 2D sample placement on the surface of the microprobe. The third dimension can be incorporated by varying the encapsulation layer thickness and thereby the distance from the microcoil turns to the microprobe surface. This provides the possibility to do more advanced sensitivity and spin excitation uniformity optimization by finding the most advantageous spots for sample placement in all three dimensions.

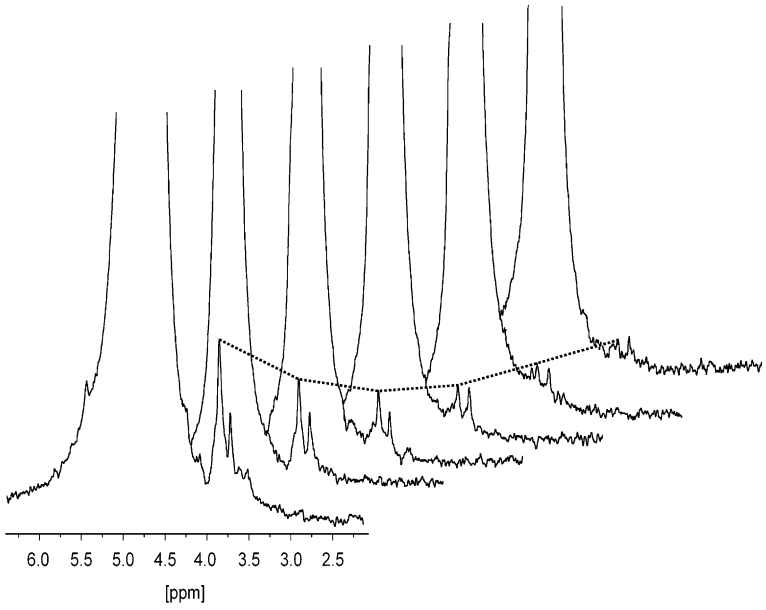

Fig. 12. Spectra of echoes returned by a CPMG spin echo excitation. Every second echo is recorded. An exponential weighting function with $LB = 4$ Hz is applied to the FID. The baseline of the spectra is corrected. A line connects the H-6 peaks of the echoes to illustrate the exponential decrease of the signal amplitude.

5.2. Potential for analysis of living cells

Lipid vesicles are used as cell substitutes to characterize the NMR surface microcoil. As the final objective is analysis of living cells, the micro-engineering techniques chosen for the immobilization and patterning of lipid vesicles, allow the immobilization and patterning of living cells as well. When patterning living cells, usually extracellular matrix is printed onto a surface [24,25]. On SU-8, some cell species even immobilize directly without any surface treatment or deposition of extracellular matrix. In these cases, substances that repel cells would be printed to create cell patterns. The use of NMR surface microcoils offers not only the possibility to immobilize living cells on its surface during the time of analysis, but also to grow and manipulate them there. Doing this, the cells could be analyzed in their natural environment without the need to harvest them before analysis.

Within living cells, the most prevalent compounds have concentrations of some 10 mM. With respect to this, the surface microcoil having a LOD_c of 300 mM with a detection volume of 1.2 nL is not sensitive enough. However, the limits of detection can be increased by several means. Optimizing the repetition time (here 7 s per scan), a factor 2 in time and a factor 1.4 in *SNR* can easily be achieved. Following the trend of high field spectroscopy and going from 300 to 900 MHz would further increase the sensitivity by a factor 6.8 ($SNR \propto \mathbf{B}_0^{7/4}$ [11]). In total, the LOD_c would decrease to about 30 mM per equivalent proton and analysis of living cells becomes possible. Many compounds within living cells have not only one but several equivalent protons, which leads to a further increase of the *SNR*.

6. Conclusions

We use aligned microcontact printing to pattern the sample on the microprobe surface in regions of homogeneous $\mathbf{B}_1$-field and high sensitivity close to the planar NMR microcoil. The spin excitation uniformity is improved drastically and achieves values in the range of conventional NMR macroprobes. Using lipid vesicles as cell substitutes and a theoretic model based on 3D finite element simulation, the microprobe performance with respect to sensitivity and spin excitation uniformity is determined. *SNR* and nutation curves of the experiments are precisely predicted.

The presented NMR surface microprobe is designed for cell analysis and the sample patterning technique is compatible with the patterning of living cell. This technique and the results of the presented NMR experiments open the way to immobilize, pattern and grow living cells on NMR microprobes and to do subsequent NMR analysis.

Acknowledgment

The microcoils have been fabricated at the Center of Micro- and Nanotechnology (CMI) at EPFL. We thank the technical staff as well as Y. Pilloud and G. Vaucher for their helpful support. We thank P.-Y. Bolinger for his assistance during the creation of the lipid vesicles and B. Hinz for providing the confocal microscope to verify optically the vesicle patterns. This work is supported by the Swiss National Science Foundation (Project No. 2100-61549.00).

References

[1] H. Andersson, A. van den Berg, Microfluidic devices for cellomics: a review, Sensor. Actuat. B 92 (2003) 315–325.

[2] R.K. Gupta, NMR Spectroscopy of Cells and Organisms, CRC Press, Boca Raton, 1987.

[3] Z. Serber, V. Dötsch, In-cell NMR spectroscopy, Biochemistry 40 (48) (2001) 14317–14323.

[4] T.L. Peck, R.L. Magin, R. Kruse, M. Feng, NMR microspectroscopy using 100 μm planar RF coils fabricated on gallium arsenide substrates, IEEE Trans. Biomed. Eng. 41 (7) (1994) 706–709.

[5] T.L. Peck, R.L. Magin, P.C. Lauterbur, Design and analysis of microcoils for NMR microscopy, J. Magn. Reson. B 108 (1995) 114–124.

[6] J.D. Trumbull, I.K. Glasgow, D.J. Beebe, R.L. Magin, Integrating microfabricated fluidic systems and NMR spectroscopy, IEEE Trans. Biomed. Eng. 47 (1) (2000) 3–7.

[7] C. Massin, F. Vincent, A. Homsy, K. Ehrmann, G. Boero, P.-A. Besse, A. Daridon, E. Verpoorte, N.F. de Rooij, R.S. Popovic, Planar microcoil-based microfluidic NMR probes, J. Magn. Reson. 164 (2003) 242–255.

[8] S. Eroglu, B. Gimi, B. Roman, G. Friedman, R.L. Magin, NMR spiral surface microcoils: design fabrication and imaging, Concept. Magn. Res. B 17 (2003) 1–10.

[9] B. Gimi, S. Eroglu, L. Leoni, T.A. Desai, R.L. Magin, B. Roman, NMR spiral surface microcoils: applications, Concept. Magn. Res. B 18 (2003) 1–8.

[10] C.S. Bosch, J.J.H. Ackerman, Surface coil spectroscopy, NMR-Basic Princ. Prog. 27 (1992) 3–44.

[11] D.I. Hoult, R.E. Richards, The signal-to-noise ratio of the nuclear magnetic resonance experiment, J. Magn. Reson. 24 (1976) 71–85.

[12] C. Massin, G. Boero, F. Vincent, J. Abenhaim, P.-A. Besse, R.S. Popovic, High-Q factor RF planar microcoils for micro-scale NMR spectroscopy, Sensor. Actuat. A 97–98 (2002) 280–288.

[13] D. Stamou, C. Duschl, E. Delamarche, H. Vogel, Self-assembled microarrays of attoliter molecular vessels, Angew. Chem. 115 (45) (2003) 5738–5741.

[14] D. Chiu, C. Wilson, F. Ryttsen, A. Strömberg, C. Farre, A. Karlsson, S. Nordholm, A. Gaggar, B. Modi, A. Moscho, R. Garza-Lopez, O. Orwar, R. Zare, Chemical transformations in individual ultrasmall biomimetic containers, Science 283 (1999) 1892–1895.

[15] M.M. Hanczyc, S.M. Fujikawa, J.W. Szostak, Experimental models of primitive cellular compartments: encapsulation, growth, and division, Science 302 (2003) 618–622.

[16] R. Singhvi, A. Kumar, G.P. Lopez, G.N. Stephanopoulos, D.I.C. Wang, G.M. Whitesides, D.E. Ingber, Engineering cell shape and function, Science 264 (1994) 696–698.

[17] B. Michel, A. Bernard, A. Bietsch, E. Delamarche, M. Geissler, D. Juncker, H. Kind, J.-P. Renault, H. Rothuizen, H. Schmid, P. Schmidt-Winkel, R. Stutz, H. Wolf, Printing meets lithography: soft approaches to high-resolution patterning, IBM J. Res. Dev. 45 (5) (2001) 697–719.

[18] C.D. James, R. Davis, M. Meyer, A. Turner, S. Turner, G. Withers, L. Kam, G. Banker, H. Craighead, M. Isaacson, J. Turner, W. Shain, Aligned microcontact printing of micrometer-scale poly-L-lysine structures for controlled growth of cultured neurons on planar microelectrode arrays, IEEE Trans. Biomed. Eng. 47 (1) (2000) 17–21.

[19] L. Lauer, S. Ingebrandt, M. Scholl, A. Offenhaeusser, Aligned microcontact printing of biomolecules on microelectronic device surfaces, IEEE Trans. Biomed. Eng. 48 (7) (2001) 838–842.

[20] K. Mouthaan, R. Tinti, M. de Kok, H.C. de Graaff, J.L. Tauritz, J. Slotboom, Microwave modelling and measurement of the self- and mutual inductance of coupled bondwires, Proceedings of Bipolar/BiCMOS Circuits and Technology Meeting (1997) 66–169.

[21] P.T. Callaghan, Principles of Nuclear Magnetic Resonance Microscopy, Clarendon Press, Oxford, 1991.

[22] K.R. Minard, R.A. Wind, Picoliter ^{1}H NMR spectroscopy, J. Magn. Reson. 154 (2002) 336–343.

[23] R.R. Ernst, G. Bodenhausen, A. Waukun, Principles of Nuclear Magnetic Resonance in One and Two Dimensions, Clarendon Press, Oxford, 1987.

[24] R.S. Kane, S. Takayama, E. Ostuni, D.E. Ingber, G.M. Whitesides, Patterning proteins and cells using soft lithography, Biomaterials 20 (1999) 2363–2376.

[25] E. Ostuni, R. Kane, C.S. Chen, D.E. Ingber, G.M. Whitesides, Patterning mammalian cells using elastomeric membranes, Langmuir 16 (2000) 7811–7819.